

## Thermally enhanced membrane gas separation



Shohei Nakaya<sup>a</sup>, Hiroshi Sugimoto<sup>a,\*</sup>, Naveen K. Gupta<sup>b</sup>, Yogesh B. Gianchandani<sup>b</sup>

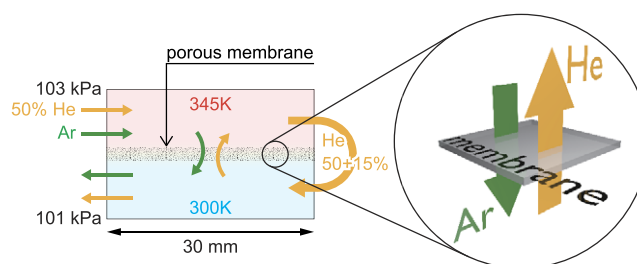
<sup>a</sup> Department of Aeronautics and Astronautics, Kyoto University, Block C3, Kyoto Daigaku Katsura, Kyoto 615-8540, Japan

<sup>b</sup> Center for Wireless Integrated Micro Sensing and Systems (WIMS<sup>2</sup>), University of Michigan, EECS Building, 1301 Beal Avenue, Ann Arbor, MI 48109-2122, USA

### HIGHLIGHTS

- Novel gas separation with temperature and pressure differences across the membrane.
- Molecular exchange flow by the thermal transpiration in the porous membrane.
- Low cost membrane is available for gas separation.
- 15% gain of mole percentage by a membrane of  $3 \times 3$  cm size with 45 K temperature difference.

### GRAPHICAL ABSTRACT



### ARTICLE INFO

#### Article history:

Received 9 October 2013

Received in revised form

14 July 2014

Accepted 14 July 2014

Available online 21 July 2014

#### Keywords:

Membrane gas separation

Thermal transpiration

Molecular gas dynamics

Rarefied gas

Porous membrane

Knudsen pump

### ABSTRACT

An enhancement of membrane gas separation, which makes use of the temperature difference in addition to the pressure difference across the porous membrane, is proposed. The thermal transpiration flow through the membrane induced by the temperature difference enables control of two physical quantities of the permeate flow, since the temperature difference is controllable separately from the pressure difference. It is possible to establish the molecular exchange state of the permeate flow, where a component gas of binary mixture flows in the opposite direction from the flows of the other component. A model gas separation device, which makes use of the counter flow arrangement to accumulate the molecular exchange of the micro-channels in the membrane, is devised using a single mixed cellulose ester membrane of  $110 \mu\text{m}$  thickness and  $3 \times 3$  cm size. The device induces 15% variation of mole percentage of a helium–argon mixture by a temperature difference of 45 K when the speed of the counter flow is around 50 cm/s. The performance of the device is well represented by numerical simulations that use the results of molecular gas dynamics for mixture flow in micro-channels.

© 2014 Elsevier Masson SAS. All rights reserved.

## 1. Introduction

Gas separation by membranes is an attractive method, because of its simple device structure, easy operation, and high energy efficiency. A great number of research efforts have been carried out for the fabrication of separation units and membranes with appropri-

ate macroscopic and microscopic structures, including the design of molecules of the membrane [1–4]. These various implementations of membrane separation have a common, simple principle. The feed is supplied to one side of the membrane at higher pressure relative to the other side, and the gas molecules permeate according to the pressure difference. The separation occurs with the dependency of the permeation speed on molecular species. The dependency comes from the fact that the mechanism of molecular transport in the membrane is quite different from that in bulk gas: various diffusion effects such as Knudsen diffusion, molecular sieving, and solution diffusion play important roles. In these

\* Corresponding author. Tel.: +81 75 383 3772; fax: +81 75 383 3774.

E-mail addresses: [sugimoto@kuaero.kyoto-u.ac.jp](mailto:sugimoto@kuaero.kyoto-u.ac.jp), [sugimoto605@yahoo.co.jp](mailto:sugimoto605@yahoo.co.jp) (H. Sugimoto).

## Nomenclature

$\alpha$	A, B mixture component
F (R)	channel at front (rear) side of membranes
H (C)	heated (unheated) plate
subscript 1, 2	1: inlet and 2: outlet at H and C
$\varepsilon$	effective porosity of the membrane
$\theta \Delta T$	effective temperature difference
$\kappa$	Boltzmann constant
$\chi$	mole percentage of A-gas
$\chi_1$	$\chi$ of the feed mixture
$\Delta \chi$	increment of $\chi$ by separation device
$\ell_c$	mean free path of A-gas at $p_c, T_c$
$\ell_R$	mean free path of A-gas at $p_R, T_R$
$\ell^{\text{BGK}}$	mean free path in the BGK model
$\ell^S$	mean free path in the S-model
$c_R$	sound speed of A-gas at $T_R$
$D$	width of channel F and R
$d$	pore size of the membrane
$d_{\text{MCE}}$	effective pore size of the membrane
$d_m^\alpha$	diameter of $\alpha$ -molecule
$\text{Err}_Q$	$= 100 (Q_1 - Q_L) / Q$
Kn	Knudsen number in micro-channel
$L = 2dm$	length of channel F and R
$L_- (L_+)$	length of inlet (outlet) of F and R
$M_1, M_2$	mass flow controller
$m$	number of simulated micro-channels
$m^{\text{BGK}}$	mass of a molecule in the BGK model
$m^S$	mass of a molecule in the S-model
$m^\alpha$	mass of $\alpha$ -molecule
$N_p (N_T)$	nondimensional flow rate of pressure (temperature) induced flow
$n^\alpha$	number density of $\alpha$ -gas
$p_c$	pressure at $C_2$
$p_D$	pressure drop between F and R
$p_F$	pressure at the inlet of channel F
$p_R$	pressure at the outlet of R
$p_i$	pressure at gauge $P_i$ ( $i = 1, 2, 3$ )
$p^\alpha$	partial pressure of $\alpha$ -gas
$\Delta p$	$= p_2 - p_3$
$\Delta p_1$	pressure difference between $H_1 - C_2$
$\Delta p_L$	pressure difference between $H_2 - C_1$
$Q$	$= (Q_1 + Q_L) / 2$
$Q_1$	volume flux of the feed mixture
$Q_L$	volume flux at U-bend part
$Q^\alpha$	net volume flux of $\alpha$ -gas through the membrane
$Q^*$	$= Q^A + Q^B$
$S$	area of the membrane
$T_F (T_R)$	temperature at the front (rear) channel
$T_H (T_C)$	temperature of heated (unheated) plate
$\Delta T$	$= T_H - T_C$
$t$	thickness of the membrane
$V$	openings of valve $V_1$ at U-bend part
$v$	flow velocity of mixture
$v_F$	flow velocity of feed mixture

implementations, we can control only one driving parameter for the molecular transport—the pressure difference across the membrane. It means that we can control only one physical quantity of permeate flow, which may be the total molecular flux of the mixture through the membrane. As a result, we cannot control the ratio of molecular fluxes of component gases; the performance of gas separation is mostly determined by the physical and chemical properties of the membrane.

The above use of membranes, however, utilizes only a part of the ability of membranes. That is, the pressure difference is just one of the driving forces of molecular transport in the membrane. According to the results of molecular gas dynamics, which deals with the behavior of the gas with a finite mean free path of gas molecules, the temperature field may induce various steady gas flows other than natural convection [5]. These flows vanish in the continuum (i.e., small mean free path) limit, but they remain appreciable in the rarefied gas, where the size of mean free path of gas molecules is comparable to the scale of the system. The rarefied condition applies to the gas in micro-channels of porous membrane if the pore diameter is comparable to the mean free path. For these porous membranes, we have two driving forces for gas flow in the membrane, which can be controlled by two different physical parameters—pressure and temperature differences across the membrane. In this case, we can control two physical quantities of permeate flow. In the case of binary mixtures, we can control molecular flux of each component independently [6]. Thus we can change the selectivity of a given membrane. It is even possible that one component flows in the opposite direction of the flow of the other component. This is one of the keys of the thermal enhancement of membrane gas separation presented in this paper.

Although there are various kinds of temperature induced flows, only a few of them can be used owing to the limitations in fabrication. The local flow speed of thermal edge flow [7,8] is proportional to the square root of the mean free path, but the requirement for the shape of micro-channel is not simple. As for the flows whose speed is proportional to the mean free path, two types of flow are investigated: the nonlinear thermal stress flow [9] and the thermal transpiration (or thermal creep) flow [10,11]. The former requires a larger variation of temperature, which is difficult to achieve in the membrane. The latter is well known linear effect and is extensively studied by many researchers, including the case for gas mixtures [10–21]. (Please refer reviews [22–24] for extensive references.) The studies lead the development of the pump with no moving parts—Knudsen pump [25]. In 2011, Gupta and Gianchandani [26] succeeded to induce the thermal transpiration flow under atmospheric pressure by using a mixed cellulose ester (MCE) membrane. Their dime-sized pump induces appreciable gaseous flux around 1 sccm and a pressure difference around 1 kPa with a temperature difference of 30 K. The pump is also stable to work continuously over 6 months. It is one crucial step for membrane technology to utilize the thermal transpiration flow. In the present paper, we make use of the design of the pump by Gupta and Gianchandani to devise our gas separation device.

The purpose of our device is to demonstrate the enhancement of membrane separation by a temperature field. The native gas separation effect of small portion of MCE membrane with temperature difference around 30 K is, of course, expected so small for engineering purposes. Some improvements are required to amplify the effect: e.g., the use of long tube [27] or a series connection of Knudsen pump [28]. In the present paper, we apply one of the existing methods of membrane gas separation. That is, we use the counter flow setup similar to the hollow fiber membrane gas separation unit [1]. This is the second key of the present work, which enables the detection of the thermal enhancement of membrane separation. First we will carry out numerical simulations on the gas flow in the test device to confirm the effect of the combination of the thermal enhancement and the counter flow setup. Second we will carry out experiments with binary mixtures of noble gases to demonstrate the new method of membrane gas separation.

## 2. Structure of gas separator

### 2.1. Concept

The schematic of our gas separator [29,30] is shown in Fig. 1. The device consists of a porous membrane with micro-channels and

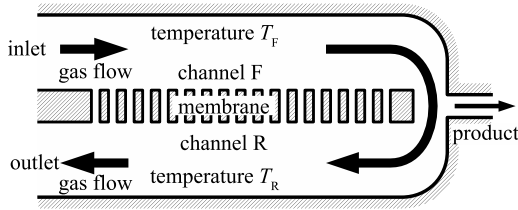


Fig. 1. Schematic of the gas separator.

two channels (F and R) along the both sides of it. The channel F is connected to the channel R at the end to form a U-bend. Feed gas, a binary gas mixture of smaller molecules A (mass of a molecule  $m^A$ ) and relatively larger molecules B (mass  $m^B$ ), is introduced into the device through the inlet. The mixture mainly flows through the channel F, the U-bend, and the channel R toward the outlet, while some part of the mixture flows through the micro-channels in the membrane. The latter flow is in the rarefied gas regime, and its nature differs from that of the flows in channels F and R. Its molecular transport generally depends on species or molecular mass, and the temperature field induces a distinctive flow of rarefied gas [5], which can be controlled by the difference between the temperature at channel F ( $T_F$ ) and that at R ( $T_R$ ). As is described in the next paragraph, it is possible that the smaller molecules A flow in the direction of R to F, while the larger molecules B flow from F to R. These species dependent flows lead to a variation of the composition of the gas in channels F and R around each individual micro-channel. Let us consider the variation of mole percentage  $\chi$  in channels F and R, which is defined by

$$\chi = \frac{100n^A}{n^A + n^B},$$

where  $n^\alpha$  ( $\alpha = A, B$ ) are, respectively, the number densities of  $\alpha$ -molecules. An increase of  $\chi$  in channel F leads to the decrease of  $\chi$  in R and vice versa, if the difference of  $\chi$  between channels F and R is small. These variations of mole percentage  $\chi$  are convected downstream of channels F and R. When all micro-channels give similar impacts on  $\chi$ , a gradient of  $\chi$  along the membrane will be induced by the accumulation. The counter flow setup in channels F and R is devised for this purpose. In this arrangement, the signs of the variations of  $\chi$  along the membrane are the same in channels F and R. This helps the difference of  $\chi$  between F and R keep small over the entire surface of the membrane so that diffusion in the micro-channels does not hinder the flows in the micro-channels. The gradient of  $\chi$  along the membrane means that a gas component is concentrated at the part of U-bend. The product of the device is a small amount of gas taken from the U-bend part.

Now we discuss the rarefied gas flow through individual micro-channels. Since the flow speed in the micro-channel is small, linear theory of the Boltzmann equation applies and the flow is shown to be induced by the gradients of pressure, temperature, and mole fraction [15]. The pressure driven flow corresponds to the Poiseuille flow, where the gas flows in the direction opposite to the pressure gradient. The thermal transpiration is the flow in the direction of the temperature gradient. The last one is the effect of diffusion. Here we estimate the gas flow in the micro-channel induced only by the pressure and temperature gradients, since, as is described in the previous paragraph, the difference of mole percentage  $\chi$  between F and R is small in normal operations of the present device. First we consider the case where the value of the temperature ratio  $T_F/T_R$  is close to that of the pressure ratio  $p_F/p_R$  ( $p_F$ : pressure at the inlet,  $p_R$ : pressure at the outlet. Note that  $p_F/p_R > 1$ ). The thermal transpiration occurs in the direction of  $R \rightarrow F$ , and the pressure driven flow is in the direction of  $F \rightarrow R$ . The main parts of these flows cancel out each other due to the condition  $T_F/T_R \approx p_F/p_R$ , and the species dependence of the flows

become important. For temperature driven flow, A-gas flows faster than B-gas, and the speed ratio is given approximately by the speed ratio of the molecules  $\sqrt{m^B/m^A}$ . This reflects the fact that thermal transpiration is characteristic to rarefied gas and is the effect of the free motion of molecules [31]. The situation is not the same for pressure driven flow. The speed ratio is  $\sqrt{m^B/m^A}$  only in the Knudsen (or large mean free path) limit. It approaches unity in the continuum limit where the free motion of molecules is intercepted by intense intermolecular interactions. The speed ratio generally takes an intermediate value between unity and  $\sqrt{m^B/m^A}$ . The difference between the speed ratios of pressure and temperature driven flows is important—it enables the arbitrary speed ratio between A-gas and B-gas in the linear combination of temperature and pressure driven flows. In the present setup  $T_F/T_R \approx p_F/p_R > 1$ , A-gas tend to flow in the direction of  $R \rightarrow F$ , more than B-gas. It is possible that A-molecules move in the direction  $R \rightarrow F$  while the same number of B-molecules move in the direction  $F \rightarrow R$  under an appropriate value of the gradients of pressure and temperature along the micro-channel [6]. Hereafter this state is referred to as “molecular exchange” in the present paper. If the pressure gradient is larger (smaller) than the appropriate value, the flows are accelerated in the direction of  $F \rightarrow R$  ( $R \rightarrow F$ ). Nevertheless A-gas has larger velocity in the  $R \rightarrow F$  direction. Finally, we consider other cases,  $T_F/T_R \leq 1$  or the thermal transpiration is very weak. In these cases, both of A-gas and B-gas flow in the direction  $F \rightarrow R$ , and the speed is larger for A-gas. The thermal transpiration enhances the effect of pressure-driven flow.

The behavior of the each component gas in the present device is exaggerated in Fig. 2. The panel (a) shows the case of  $T_F/T_R > 1$ . The B-molecules are exhausted from the device by the flow  $F \rightarrow R$ , while some part of A-molecules circulate around the U-bend part by the flow  $R \rightarrow F$  through the membrane. Therefore, A-gas is concentrated in the product gas. The panel (b) shows the case of  $T_F/T_R \leq 1$ . A-molecules are exhausted from the device earlier than B-molecules, and the product gas is B-rich. The case of  $T_F/T_R = 1$  is the same as the membrane gas separator by Knudsen diffusion. The thermal transpiration flow in the  $F \rightarrow R$  direction for  $T_F/T_R < 1$  will intensify this effect.

The expression of the increment  $\Delta\chi$  of the mole percentage of the product gas is obtained with the mass conservation as

$$\Delta\chi = \frac{(100 - \chi_1) Q^A - \chi_1 Q^B}{Q_1 + Q^A + Q^B},$$

where  $Q_1$  and  $\chi_1$  are, respectively, the volume flux and mole percentage of the feed, and  $Q^\alpha$  are the net volume flux of  $\alpha$ -gas through the membrane in the  $R \rightarrow F$  direction. The sizes of  $Q^\alpha$  depend on the flow speeds in the micro-channel and partial pressures in F and R. In the case of  $T_F/T_R > 1$ , the condition  $Q^A > 0 > Q^B$  is available that ensures  $\Delta\chi > 0$ . In order to simplify the experimental procedure, we will try to establish the pure molecular exchange condition

$$Q^A + Q^B = 0, \quad (1)$$

in the present work.

## 2.2. Device structure

The exploded view and the photograph of fabricated device are shown in Fig. 3. The cross section and closeup figures are also shown in Fig. 4. Two aluminum plates H and C sandwich several sheets including the thermal transpiration membrane, which are described later. A small heater unit [ $10 \times 10 \times 1$  mm, Micro Ceramic Heater MS-3 (Sakaguchi E.H VOC Corp.) with rated heating power 40 W] is attached between plate H and the top cover U (aluminum,  $50 \times 50 \times 3$  mm). Heat-dissipating silicone grease is applied

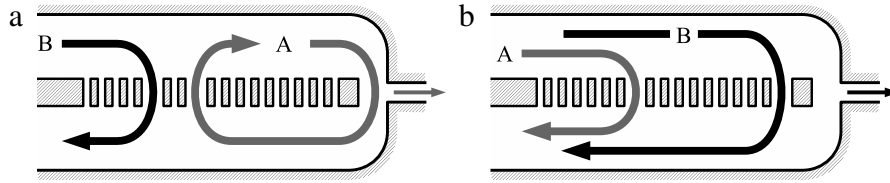


Fig. 2. Behavior of the component gas in the gas separator. A: gas with smaller mass of a molecule. B: that for larger mass of a molecule. (a)  $T_F/T_R > 1$ ; (b)  $T_F/T_R \leq 1$ .

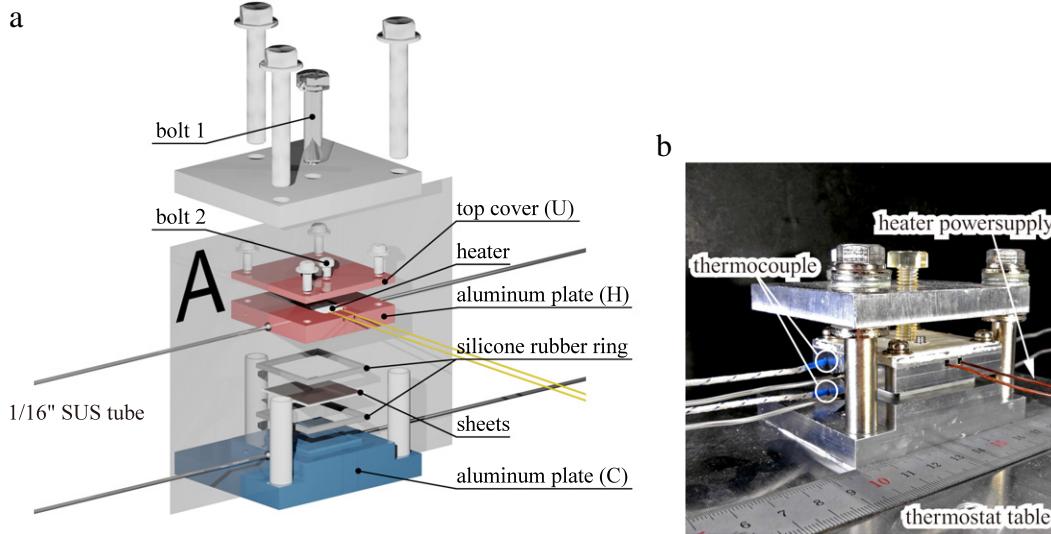


Fig. 3. (a) Exploded view of the device. (b) The photograph of the device. The cross section at plane A of the device is shown in Fig. 4(b).

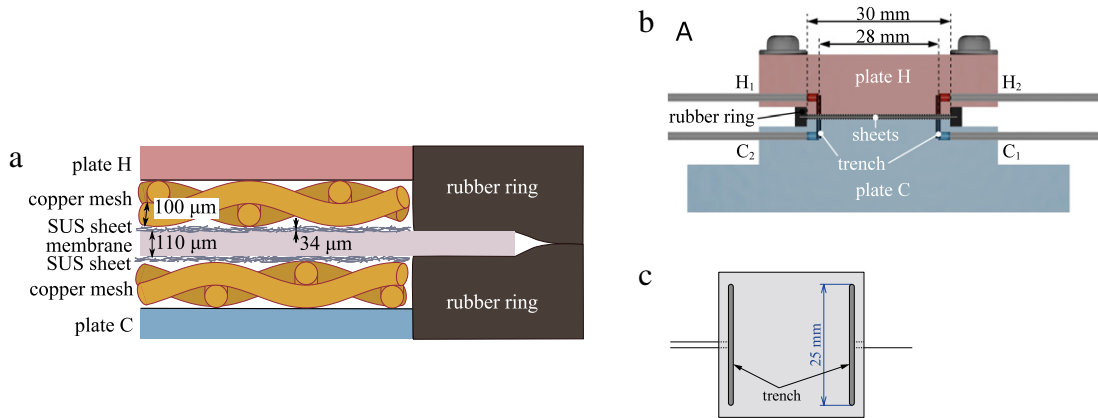


Fig. 4. Cross sections of the device. (a) Close up of multilayered mesh structure. (b) Gas inlet and outlet system. (c) Top view of the stage for the sheets.

between the heater and plate H, and the heater is held against the plate H. The heat supplied by the heater is removed from plate C, which will be fixed to the thermostat table as shown in Fig. 3(b). The temperatures of plate H ( $T_H$ ) and C ( $T_C$ ) are measured by thermocouples shown in Fig. 3(b). Then we install the sheets including the membrane between plates H and C. The membrane is a mixed cellulose ester (MCE) membrane (Advantec MFS Inc. A010A047A). The pore size, thickness, and porosity of the MCE membrane are  $0.1 \mu\text{m}$ ,  $110 \mu\text{m}$ , and 65%, respectively. The size of the MCE membrane is  $33 \times 33 \text{ mm}$ . This MCE membrane is a standard filter membrane, and about  $10^3$  times thicker than those used in usual membrane gas separation. Two flow channels F and R along the MCE membrane are required according to the concept given in Section 2.1. This is done by the multilayered mesh structure as in [32,33]. That is, the MCE membrane is sandwiched between two sintered SUS fiber sheets ( $30 \times 30 \text{ mm}$ , thickness

$34 \mu\text{m}$ , and the porosity is around 80%. Tomoegawa Paper Co. Ltd., Tomifleck SS8-50M) [see Fig. 5(a)], which is composed of short fiber of SUS316 with diameter  $8 \mu\text{m}$ . Then it is sandwiched by two copper meshes of size  $30 \times 30 \text{ mm}$  [thread diameter  $100 \mu\text{m}$ , #100, see Fig. 5(b)]. The copper meshes provide the gas flow channel along the both sides of the MCE membrane, and SUS sheets protect the MCE membrane [Fig. 4(a)]. These metal meshes also provide the heat flux from plates H and C to MCE surfaces. The edges of the MCE membrane are sealed by two square silicone rubber square rings (outer size  $35 \times 35 \times 2 \text{ mm}$ , inner size  $30 \times 30 \times 2 \text{ mm}$ ) as shown in the right end of Fig. 4(a).

The inlet and outlet for the gas flow are prepared as two trenches ( $25 \times 1 \text{ mm}$ , depth  $4 \text{ mm}$ ) on the stage part of plates H and C [see Fig. 4(c)]. The gas is supplied and exhausted through the  $1.7 \text{ mm}$  diameter holes extended to the trenches in the plates H and C. For later convenience, inlets are identified by subscript 1 and outlets by 2 (e.g.,  $H_1$  is the inlet at plate H).

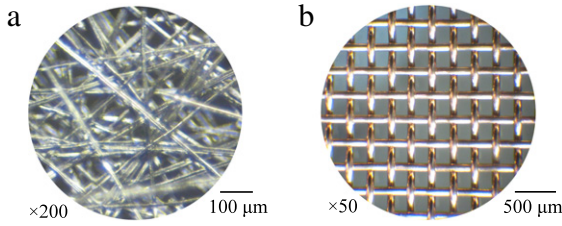


Fig. 5. Photographs of the metal meshes used in the device. (a) Sintered SUS fiber sheet and (b) copper mesh.

### 3. Performance simulation

This is the first experimental work on the gas separation with the thermal transpiration through a membrane, and there is no known result for this kind of device. Especially, the molecular exchange flow of the rarefied gas has never been confirmed experimentally. In this case, theoretical works become important to confirm the fabricated device works as expected. Therefore, in this section, we carry out numerical analysis on the behavior of the mixture in the device. The purpose of the analysis is to determine the setup of the experiment, e.g., the connection of  $H_*$  and  $C_*$  ports of the device, and to estimate the qualitative features of molar fraction, etc., expected in the experiment of the present device.

The model of the gas separator device used in the numerical simulation is shown in Fig. 6. The model is 2D in  $X_1$ - $X_2$  space, where the  $X_1$ -direction is taken along the membrane, which is replaced with an array of  $m$  micro-channels in the model (cf. Fig. 1). The width and length of each micro-channel are  $d$  and  $t$ , respectively. The spacing between the channels is  $d$ . The wall temperature in the micro-channel varies linearly from  $T_R$  (at channel R) to  $T_F$  (at channel F). The location of the array is  $0 < X_1 < L = 2dm$ . The channels R and F are slightly longer than  $L$ ; their ends are at  $X_1 = -L_-$  and  $L + L_+$ . The width of both R and F is  $D$ . The feed gas is supplied to channel F at  $X_1 = -L_-$ . The mole percentage of smaller A-gas and temperature of feed mixture is, respectively,  $\chi_1$  and  $T_F$ . The gas is removed from channel F at the other end ( $X_1 = L + L_+$ ). In the simple case with no production of gas, all of the gas is refluxed into channel R at  $X_1 = L + L_+$ , after regulating the temperature to  $T_R$  with some pressure drop  $p_D$ . The fluxes of  $\alpha$ -gas at the inlet of R are determined by those at the outlet of F. The gas leaves the device at  $X_1 = -L_-$  from channel R. The pressure, temperature, and number density of the mixture at the outlet are  $p_R$ ,  $T_R$  and  $n_R (=p_R/\kappa T_R, \kappa$ : Boltzmann constant), respectively.

In a calculation based on the kinetic theory, the size  $\ell_R$  of mean free path of gas molecules at a reference state is required to determine the impact of molecular collisions on gas motion. The mean free path of gas mixture is complicated since the sizes of free paths differ depending on the species of colliding molecules (e.g., A–A, A–B, and B–B pairs for binary mixture of A and B molecules). However, their ratios under some specific gas state are expressed by the parameters in intermolecular potentials, e.g., the diameter of molecule  $d_m^\alpha$  ( $\alpha = A, B$ ). In the present paper, we define  $\ell_R$  as the mean free path of pure A-gas at the stationary equilibrium

state with number density  $n_R$  and temperature  $T_R$ . For hard-sphere molecules,

$$\ell_R = \left[ \sqrt{2\pi} (d_m^A)^2 n_R \right]^{-1}. \quad (2)$$

Since we are interested in the phenomena in micro-channels, we specify the size of  $\ell_R$  by the Knudsen number in the micro-channel:

$$\text{Kn} = \frac{\ell_R}{d}. \quad (3)$$

Please note that Kn is not the degree of rarefaction for larger channels F and R. The local Knudsen number there is  $\text{Kn}(d/D)$ , which is much smaller than Kn since  $d \ll D$ . Incidentally, the relation between the mean free path and fluid properties such as viscosity is one of the basic problems in the kinetic theory and now we have enough informations for pure and mixture gases [22,31,34,35]. For pure A-gas of hard-sphere molecules,

$$\nu^A \approx 0.563 \sqrt{\frac{2\kappa T_R}{m^A}} \ell_R, \quad (4)$$

where  $\nu^A$  is the kinematic viscosity at pressure  $p_R$  and temperature  $T_R$  [22,31]. Since the experimental values of viscosity, etc., are available for pure gases, we can make comparison with our analytical and experimental results through (2)–(4).

From the gas dynamic point of view, the gas flow in the above model consists of flows in two different regimes. The gas in the micro-channels is in the rarefied regime since the diameter of the micro-channel is the order of the mean free path of the gas molecules. The analysis with the Boltzmann equation is essential, since the driving mechanism of the present device makes use of the phenomena characteristic to rarefied gas. Conversely the flows in channels R and F are in the continuum regime due to the large width of the channel. Although the Boltzmann equation is able to describe the gas in nearly continuum regime, the large width of channels R and F does not allow us to carry out precise numerical analysis by the Boltzmann equation for whole device.

One of the solutions for analyzing the gas flow in this device is the “pipenet method” proposed in our previous paper [29]. This is a method similar to one used to analyze the membrane gas separation performance [36] except for the micro-channel. In the pipenet method, we pay attention only to the longitudinal variations of the partial pressures  $p^\alpha$  ( $\alpha = A, B$ ) of component gases in channels R and F. The temperature of the gas is assumed to be uniformly  $T_R$  in channel R and  $T_F$  in channel F. The distribution of  $p^\alpha$  is determined from mass conservation with the aid of the pre-constructed database [37] of rarefied flow through a channel. The details of the method are given in the Appendix. In [29], the performance of a small device with 50 micro channels is analyzed by two approaches: the direct simulation Monte Carlo (DSMC) method [38] of the Boltzmann equation and the proposed pipenet method. It is shown that the pipenet method reproduces the DSMC results with smaller CPU time (the ratio of CPU time  $> 10^5$ ). In view of this result, we apply the pipenet method to estimate the performance of the present device.

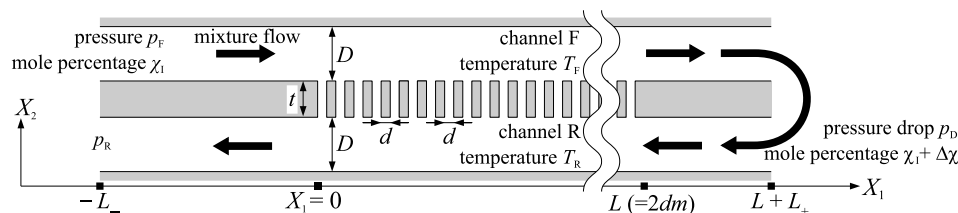
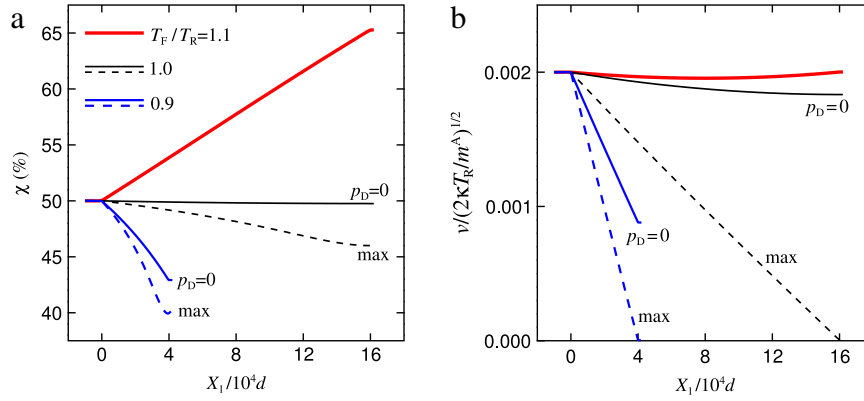


Fig. 6. Numerical model of the device.



**Fig. 7.** Result of numerical simulations for gas separators with  $T_F/T_R > 1$  and  $T_F/T_R \leq 1$ .  $m^B/m^A = 2$ ,  $\text{Kn} = 0.5$ ,  $t/d = 10^2$ ,  $D/d = 2 \times 10^3$ , and  $v_F/c_R = 2 \times 10^{-3}$ . The results for  $T_F/T_R = 0.9, 1, 1.1$ . Two extreme cases for  $p_D/p_R$  are shown for the cases  $T_F/T_R \leq 1$ . The distribution of (a) mole percentage  $\chi$  of A-gas and (b) the flow velocity  $v$  of mixture in the  $X_1$  direction.

### 3.1. Gas separators for $T_F/T_R > 1$ and $T_F/T_R \leq 1$

First we assess the possibility of two types of device given in Section 2.1,  $T_F/T_R > 1$  and  $T_F/T_R \leq 1$ , based on the results shown in [29]. The analysis is carried out for binary mixture of hard sphere molecules A and B with the same molecular diameter. The mass ratio  $m^B/m^A = 2$ ,  $\chi_1 = 50\%$ ,  $\text{Kn} = 0.5$ ,  $t/d = 10^2$ , and  $D/d = 2 \times 10^3$ . The simulation is carried out for  $T_F/T_R = 0.9, 1, 1.1$ , and the value of  $m$  is determined depending on the situation. The pressure ratio  $p_F/p_R$  is determined so that the flow speed  $v_F$  at inlet ( $X_1 = -L_-$  in channel F) satisfies  $v_F/c_R = 2 \times 10^{-3}$ , where  $c_R = (2\kappa T_R/m^A)^{1/2}$  is the reference thermal velocity of A-molecules. Another parameter is the value of pressure drop  $p_D/p_R$ , which determines the flux through the membrane  $Q^A$ . In the case of  $T_F/T_R = 1.1$ , it is possible to use (1) to determine the value of  $p_D/p_R$ . For other cases,  $T_F/T_R = 1$  and  $0.9$ , the solutions are parameterized by  $p_D/p_R$ .

Fig. 7 shows the distribution of mole percentage  $\chi$  of smaller molecules A [panel (a)] and average flow velocity  $v$  of the mixture [panel (b)] in channel F along the  $X_1$  axis. The values of  $\chi$  and  $|v|$  in channel R are very close to those in F. The number of micro-channels  $m = 8 \times 10^4$  for  $T_F/T_R = 1, 1.1$  and  $m = 2 \times 10^2$  for  $T_F/T_R = 0.9$ . The solutions depend on  $p_D/p_R$  for  $T_F/T_R \leq 1$ , and thus two extreme cases are shown in the figure. As is expected in Section 2.1, for the case of  $T_F/T_R = 1.1$ , the mole percentage  $\chi$  increases with  $X_1$  while the flow velocity  $v$  is almost constant. Conversely, the value of  $\chi$  decreases with  $X_1$  for  $T_F/T_R \leq 1$ . The amount of decrease gets larger as pressure drop  $p_D/p_R$  increases, since the size of the molecular flow through the membrane increases. However, large molecular flow through the membrane leads to small downstream flow speed in channel F. There is an upper limit for the value of  $p_D/p_R$ , where the flow velocity  $v$  vanishes at  $X_1 = L + L_+$ . This state is shown by label “max” in Fig. 7. In both cases,  $p_D = 0$  or max, it is impossible to extend the membrane to obtain larger variation of  $\chi$ . We are not free from the drop of flow velocity  $v$  for intermediate values of  $p_D/p_R$ . In view of these results,  $T_F/T_R < 1$  is impossible in the present device since we have small amount of gas at U-bend part ( $X_1 = L + L_+$ ). The performance of the case with  $T_F/T_R = 1$ , which corresponds the membrane gas separator with Knudsen diffusion, is limited: both of the variation of mole percentage and the gas flow at U-bend part may remain small. This low performance explains why other mechanisms, such as solution diffusion [1–3], are applied in the main stream of the membrane gas separation. The case with  $T_F/T_R > 1$  is promising since we have appreciable variation of mole percentage, and the flow does not vanish at U-bend part. In this case, we may extend the membrane to obtain larger variation of  $\chi$ . Indeed other numerical simulations with larger number of micro-channels  $m = 5 \times 10^5$  show larger

variation of  $\chi$ :  $\chi_1 + \Delta\chi = 96\%$  for  $\chi_1 = 10\%$ ,  $\chi_1 + \Delta\chi = 99.98\%$  for  $\chi_1 = 95\%$ , and  $\chi_1 + \Delta\chi = 12.5\%$  for  $\chi_1 = 0.1\%$ . We do not find any restriction for mole fraction for this device. This is the effect of molecular exchange condition (1).

In view of these results, we will carry out the experiments for  $T_F/T_R > 1$ . That is, the heated part H (unheated part C) of the fabricated device shown in Section 2.2 corresponds to channel F (channel R) in Section 2.1.

Before proceeding further, we have to discuss the molecular model for gas mixtures. The present model – hard-sphere molecules with the same diameter – is so simple that can cause quantitative disagreement between the theoretical and experimental results. Instead, the basic concept in Section 2.1 of the gas separation, which is based on the difference of mass of molecules of any gas mixture, is well embodied by this simple model. The effect of realistic model can be confirmed by separate numerical simulation for specific gas mixture. It is easy to carry out the test since database [37] provides the data for various intermolecular potentials, just in the same formulation proposed in [19,20]. In the case with Lennard-Jones (LJ) model of Ne–Ar mixture ( $m^B/m^A \approx 2.0$ ) at  $T_F = 330$  K,  $T_R = 300$  K,  $m = 5 \times 10^4$ ,  $t/d = 100$ ,  $D/d = 500$ ,  $\chi_1 = 50\%$ ,  $\text{Kn} = 0.5$  and  $v_F/c_R \approx 2.1 \times 10^{-3}$ , the value of  $\Delta\chi$  is around 25%, while the corresponding hard-sphere (HS) result with  $m^B/m^A = 2$  and  $d_m^A = d_m^B$  is  $\Delta\chi \approx 27\%$ . Except the value of  $\Delta\chi$ , we find various quantitative differences between LJ and HS results. For example, the value of pressure drop  $p_D/p_R$  is  $p_D/p_R = 0.012$  for LJ and  $0.005$  for HS, the net volume flux  $Q^A$  through the micro channels for HS is almost twice of that for LJ. However, it is clear that the HS model gives qualitatively the same result with the realistic LJ model. In this paper, we choose a simpler hard-sphere model for present 2D simulation, which aims to estimate the qualitative feature of the fabricated device for various gas mixtures.

### 3.2. Performance simulation

Now we carry out the numerical simulation for the fabricated device described in Section 2.2. The mass ratio is  $m^B/m^A = 10$ , which corresponds to the helium–argon mixture used in the experiments in the next section. According to the product specification of the MCE membrane and the mean free path of helium molecules under atmospheric pressure, we select  $\chi_1 = 50\%$ ,  $\text{Kn} = 2$ ,  $t/d = 10^3$ ,  $D/d = 2 \times 10^3$ , and  $m = 1.5 \times 10^5$ . The molecular model is the hard sphere molecules with the same diameter of molecules.

First we analyze the effect of the flow speed over the membrane, since the present device depends on the convection in channels F and R. If there were no convection effects, the outflows of

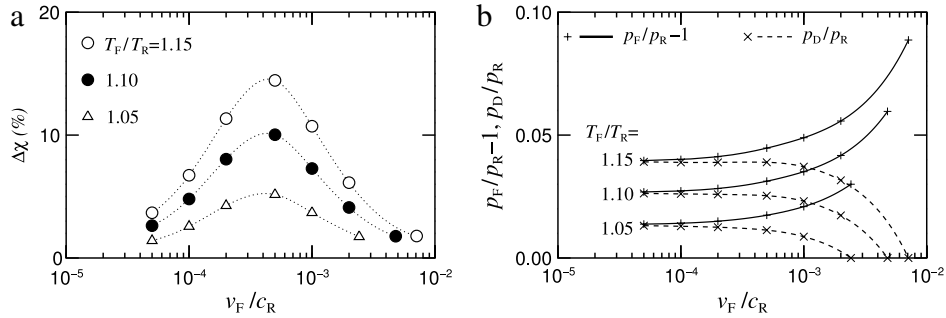


**Fig. 8.** Result of numerical simulation for the fabricated device. Effects of the flow speed  $v_F/c_R$  and the temperature ratio  $T_F/T_R$ .  $m^B/m^A = 10$ ,  $Kn = 2$ ,  $t/d = 10^3$ ,  $D/d = 2 \times 10^3$ , and  $L/d = 3 \times 10^5$ . (a) The gain of mole percentage  $\Delta\chi$ , and (b) the pressure ratio  $p_F/p_R - 1$  and the pressure drop  $p_D/p_R$  versus  $v_F/c_R$ . The results for  $T_F/T_R = 1.05, 1.1, 1.15$ .

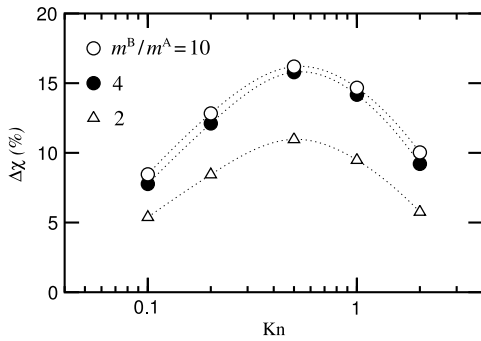


**Fig. 9.** The numerical results of the gain of mole percentage. The effect of the Knudsen number  $Kn$  and mass ratio  $m^B/m^A$ .  $T_F/T_R = 1.1$ ,  $v_F/c_R = 5 \times 10^{-4}$ ,  $t/d = 10^3$ ,  $D/d = 2 \times 10^3$ , and  $L/d = 3 \times 10^5$ .

the micro-channels in F and R may diffuse upstream and downstream without distinction. Fig. 8(a) shows the gain of mole percentage  $\Delta\chi$  for various values of  $v_F/c_R$ . The results are shown for  $T_F/T_R = 1.05, 1.1, 1.15$ . It is clear that  $\Delta\chi$  become smaller for smaller values of  $v_F/c_R$ . Smaller  $v_F/c_R$  leads to larger diffusion in channels F and R, and this causes larger difference of  $\chi$  between channels R and F at the same  $X_1$ . Then the molecular exchange flow through the micro-channels is choked by the diffusion in micro-channels. For larger values of  $v_F/c_R$ , the effect of molecular exchange flow is diluted by larger fluxes in channels F and R, which result in smaller gain of mole percentage. As a result, the value of  $\Delta\chi$  takes a maximum value at an intermediate value of  $v_F/c_R$ . Its value is  $v_F/c_R \approx 0.05$ , which corresponds to  $v_F \approx 60$  cm/s for helium–argon mixture. It is noted that molecular exchange flow does not vanish for larger values of  $v_F/c_R$ ; the numerical data shows that the values of  $Q^A (= -Q^B)$  increase and approach some upper bounds as  $v_F/c_R$  increases. There is, however, an upper limit for  $v_F/c_R$ , since larger flow speed induces larger pressure drop along channels F and R. The values of pressure ratios  $p_F/p_R$  and  $p_D/p_R$  are shown in Fig. 8(b) versus  $v_F/c_R$ . For larger values of  $v_F/c_R$ , the values of  $p_F/p_R$  increase to establish the prescribed flow speed. This leads to smaller values of  $p_D/p_R$ , since we are restricted to molecular exchange state (1). That is,  $p_D = 0$  gives the upper limit of  $v_F/c_R$ . While the solution does not exist for larger values of  $v_F/c_R$  depending on  $T_F/T_R$ , the value of  $\Delta\chi$  shows almost linear dependence on  $T_F/T_R - 1$  around  $v_F/c_R \approx 10^{-3}$ . This relation will be confirmed in the experiment in Section 4.3.

We also carried out the performance simulation for various values of Knudsen number  $Kn$  and mass ratio  $m^B/m^A$ . The values of  $\Delta\chi$  versus  $Kn$  are plotted for  $m^B/m^A = 2, 4, 10$ . The temperature ratio  $T_F/T_R = 1.1$  and flow speed is  $v_F/c_R = 5 \times 10^{-4}$ . The values of other parameters are the same as those used in Fig. 8. The values of  $\Delta\chi$  takes its maximum value at  $Kn \approx 0.5$  for any value of  $m^B/m^A$ . The maximum at intermediate  $Kn$  corresponds to the

feature of the molecular exchange flow (cf. Section 2.1) through the micro-channels. In the continuum limit  $Kn \rightarrow 0$ , the thermal transpiration thus the molecular exchange vanishes. In Knudsen limit  $Kn \rightarrow \infty$ , the speed ratio of A-gas to B-gas is  $\sqrt{m^B/m^A}$  for Poiseuille and thermal transpiration flows. In this case the speed ratio is  $\sqrt{m^B/m^A}$  for any linear combination of these flows; the molecular exchange is impossible. As the result, the size of molecular exchange flow takes a maximum value at an intermediate Knudsen number [6]. It is noted that  $\Delta\chi$  for  $m^B/m^A = 4$  and 10 are almost the same. As is discussed above, the speed of molecular exchange flow is determined by the difference of the species-dependency of Poiseuille and thermal transpiration flows at intermediate Knudsen numbers. Therefore it is natural that the dependence of the speed of molecular exchange flow on  $m^B/m^A$  is complicated.

## 4. Experimental results

### 4.1. Performance test setup

The measurement apparatus is shown in Fig. 10. The gas mixture is fed to inlet  $H_1$  of the test device. The outlet  $H_2$  is connected to inlet  $C_1$  via a needle valve  $V_1$ . The outlet  $C_2$  is open to atmospheric environment. The volume flux of the feeding is denoted by  $Q_I$ , and that of the loop part  $H_2 \rightarrow C_1$  by  $Q_L$ . The size of  $Q_L$  is controlled by two mass flow controllers  $M_1$  [Horiba STEC SEC-400 (FS 100 sccm)] and  $M_2$  [Horiba STEC SEC-400 (FS 50 sccm or 1000 sccm, depending on the size of  $Q_L$ )]. The volume flux at the loop part  $H_2 \rightarrow C_1$ ,  $Q_L$ , is controlled by  $V_1$ , which may be Swagelok SS-SS1 or SS-2MG depending on the size of  $Q_L$ . For several cases with large value of  $Q_L$ , we remove the valve  $V_1$  and control the flux by the length of the tubing. All part of these connections are done by the stainless tube with inner diameter 1 mm. Three differential pressure sensors [Honeywell ASDXRRX010NGAA5 (FS 2.5 kPa) or Freescale Semiconductor MPX2053 (FS 50 kPa)]  $P_1, P_2$ , and  $P_3$  are connected, respectively, around  $H_1, H_2$ , and  $C_1$  to obtain the differential pressure from the environment. The pressure measured by sensor  $P_i$  will be denoted by  $p_i$  ( $i = 1, 2, 3$ ). The symbol G in the figure is a two-port gas sampling system, which can take small amount of sample gas intermittently from desired port without mixing the gases at two ports. One port is connected to  $H_1$ , and the other port is connected to  $C_1$ . The sampled gas is lead to QMS (quadrupole mass spectrometer, Pfeiffer QMS200) with a metal dosing valve (Pfeiffer UDV040) to analyze the component of the sampled gas. The device is put on a thermostat table T to keep the temperature  $T_C$  of plate C of the test device at 300 K.

It is noted that the available range of  $Q_L$  depends on the temperature difference  $\Delta T = T_H - T_C$ . In the isothermal case  $\Delta T = 0$ ,  $Q_L$  is smaller than  $Q_I$ , since some part of the feed gas flows from  $H_1$

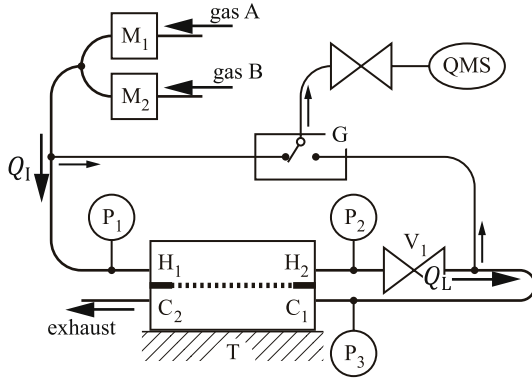


Fig. 10. Diagram of measurement system.

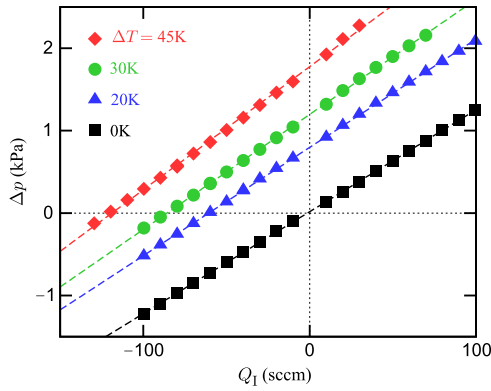


Fig. 11. Knudsen pump performance.  $\Delta p$  vs  $Q_1$  for various  $\Delta T$ . The data for 50% v/v mixture of helium and argon,  $T_c = 300$  K and atmospheric pressure at the outlet. The symbols represent the result of experiments.  $\Delta T = 0$ : black square, 20 K: blue triangle, 30 K: green circle, and 45 K: red diamond. The linear regressions are also shown in the figure.

to  $C_1$  through the membrane and does not reach  $H_2$ . In other cases,  $\Delta T > 0$ , the thermal transpiration flow in the direction  $C \rightarrow H$  expands the available range of  $Q_L$ . The value of  $Q_L$  is expressed by  $Q_1$  and  $Q^A$  introduced in Section 2.1 as follows:

$$Q_L = Q_1 + Q^A + Q^B.$$

Since we are interested in the molecular exchange state (1), we select

$$Q_L = Q_1 \quad (5)$$

in the experiment. To this end we have to measure the size of  $Q_L$ , which is obtained from the values of  $p_2$  and  $p_3$ . This is done as follows. (i) Remove the test device and replace  $H_1 \rightarrow H_2$  and  $C_1 \rightarrow C_2$  parts by straight pipes. (ii) Measure the pressure drop  $\Delta p = p_2 - p_3$  by valve  $V_1$  for various valve openings  $V$  and volume flux  $Q_1$  to construct a calibration function

$$\Delta p = h_c(V, Q_1).$$

Then we have

$$\Delta p = h_c(V, Q_L), \quad (6)$$

in the main experiments with the test device. On the other hand, the pressure difference  $\Delta p$  of main experiment with the test device is determined by  $V$ ,  $Q_1$ , and  $\Delta T$ :

$$\Delta p = \Delta p(V, Q_1, \Delta T). \quad (7)$$

Then we can determine the appropriate valve openings  $V$  from (5)–(7) for prescribed values of  $Q_1$  and  $\Delta T$ .

## 4.2. Knudsen pump performance

First of all, we have to confirm that the thermal transpiration flow through the membrane is successfully induced by the present device. To this end we shut the valve  $V_1$  for the entire supplied gas to go through the membrane. Then, we carry out the following experiment: (i) supply some electricity to the heater of the test device, and keep a constant temperature difference  $\Delta T$ ; (ii) supply gas mixture through  $M_1$  and  $M_2$  at volume flow rate  $Q_1$ ; (iii) measure the pressure difference  $\Delta p$  for various flow rates  $Q_1$ . The results for negative values of  $Q_1$  are obtained by connecting gas supply from  $M_1$  and  $M_2$  to  $C_2$  of the device with  $H_1$  being open to the atmosphere.

The experiment is carried out for 50% v/v mixture of helium and argon,  $\Delta T = 0, 20, 30$ , and 45 K. The values of electricity supplied to the heater are, respectively, 1.6 W ( $\Delta T = 0$  K), 10.0 W (20 K), 14.1 W (30 K), and 20.0 W (45 K). The electricity does not vanish at  $\Delta T = 0$  K since the environmental temperature is 286 K on average, which is lower than  $T_c = 300$  K. The value of  $\Delta p$  is plotted versus  $Q_1$  in Fig. 11. At  $\Delta T = 0$ , the pressure difference  $\Delta p$  is almost proportional to the volume flux  $Q_1$  through the device. Their relation is represented by

$$Q_1(\text{sccm}) \approx 81\Delta p(\text{kPa}) \quad (\Delta T = 0). \quad (8)$$

This is natural since the membrane has own pressure drop. As  $\Delta T$  increases, the relation is shifted; the gas flows from C part to H part ( $Q_1 < 0$ ) for  $\Delta p = 0$  and the pressure at H part is higher than that at C part ( $\Delta p > 0$ ) when the gas flow vanishes ( $Q_1 = 0$ ). This is the effect of the thermal transpiration, and the device works as a Knudsen pump in the same way as our previous work [26]. Incidentally the effect of larger viscosity for higher temperature is seen in the figure:  $dQ_1/d\Delta p \approx 70$  for  $\Delta T = 45$  K. The value of  $\Delta p$  at  $Q_1 = 0$  is the maximum pressure difference obtained by the thermal transpiration. These values are  $\Delta p = 0.80$  kPa ( $\Delta T = 20$  K), 1.20 kPa (30 K), and 1.78 kPa (45 K). These results are close to those in our previous device [26]. The size of volume flux  $Q_1$  at  $\Delta p = 0$  is the maximum volume flux obtained by the thermal transpiration. Their values are 61 sccm ( $\Delta T = 20$  K), 86 sccm (30 K), and 119 sccm (45 K). The value of flux  $Q_1$  at  $\Delta p = 0$  is roughly proportional to  $\Delta T$  and is expressed by

$$Q_1(\text{sccm}) \approx -2.8\Delta T(\text{K}) \quad (\Delta p = 0). \quad (9)$$

The value of volume flux at  $\Delta T = 30$  K is around 90 times larger than those given in [26], since the size of the membrane in the present device is around 10 times larger and the sound speed is higher with small helium molecules. These results show that the present device successfully induces the thermal transpiration flow.

## 4.3. Gas separator performance

Now we describe the main experiment of gas separation for two types of gas mixtures: (I): helium–argon 50% v/v mixture and (II): helium–neon 50% v/v mixture. The process of the experiment is as follows. (i) Keep the prescribed temperature difference  $\Delta T$  with the heater; (ii) supply the gas mixture of volume flux  $Q_1$  to the device; (iii) set the volume flux at loop part  $Q_L$  identical with  $Q_1$  with the valve  $V_1$ ; (iv) analyze the components of the gas at  $H_1$  and  $C_1$ . The detailed process of (iv) is as follows: (iv.1) repeat sampling from  $H_1$  25 times in every 3 min, and analyze the gas components by QMS; (iv.2) repeat the same analysis for  $C_1$ ; (iv.3) repeat (iv.1)–(iv.2) four times; (iv.4) finally carry out process (iv.1). In each QMS analysis, we omit first 15 data, and the average of remaining 10 data are adopted as the final result to avoid the effect of the gas left in the tubing. Thus we obtain five mole percentages  $\chi[H_1^{(n)}]$  ( $n = 1, 2, \dots, 5$ ) at  $H_1$ , and four  $\chi[C_1^{(n)}]$  at  $C_1$ , where  $\chi$

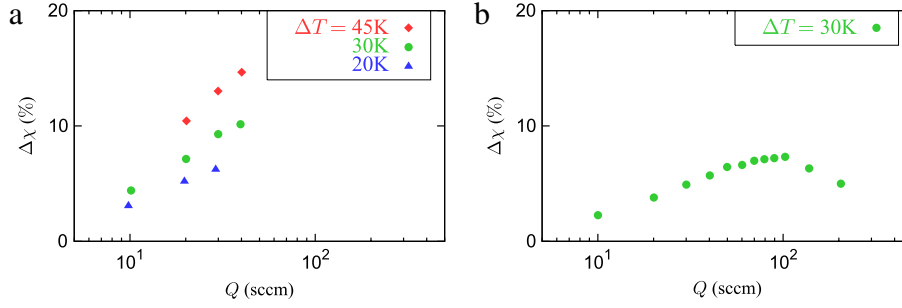


**Fig. 12.** Gas separation performance I:  $\Delta\chi$  vs  $Q$ . (a) Experiment (I) helium–argon mixture,  $\Delta T = 20, 30,$  and  $45$  K; (b) experiment (II) helium–neon mixture,  $\Delta T = 30$  K.

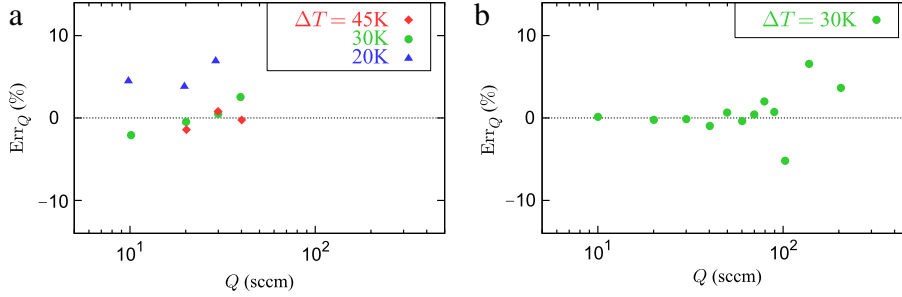


**Fig. 13.** Gas separation performance II: the value of  $\text{Err}_Q = 100(Q_L - Q_A)/Q$  vs  $Q$ . (a) Experiment (I) helium–argon,  $\Delta T = 20, 30,$  and  $45$  K; (b) experiment (II) helium–neon,  $\Delta T = 30$  K.

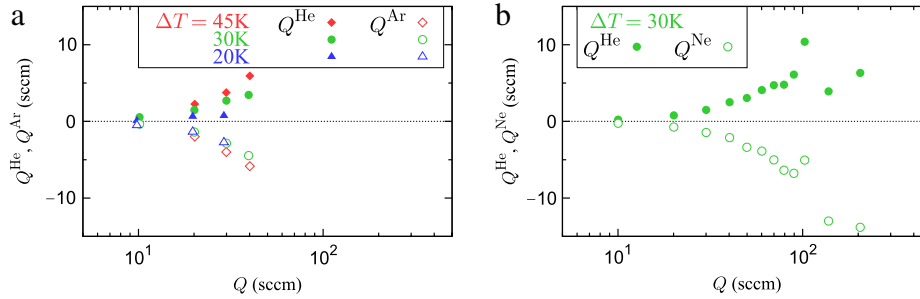


**Fig. 14.** Gas separation performance III: the value of  $Q^A, Q^B$  vs  $Q$ . (a) Experiment (I): A: helium, B: argon,  $\Delta T = 20, 30,$  and  $45$  K; and (b) experiment (II): A: helium, B: neon,  $\Delta T = 30$  K. The values of  $Q^A$  are shown by filled markers, and those of  $Q^B$  are shown by hollow markers.

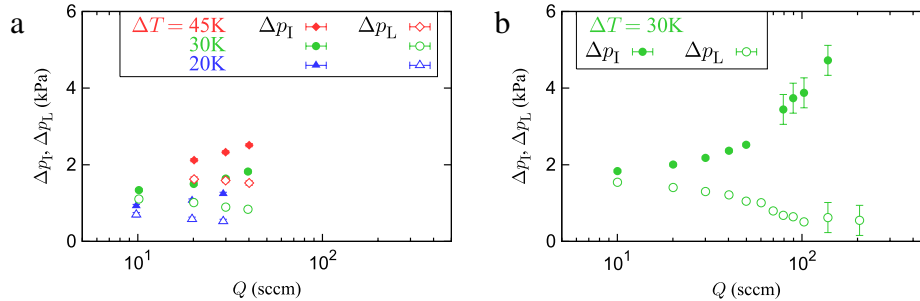


**Fig. 15.** Gas separation performance IV: the pressure differences between the membrane.  $\Delta p_I$ : filled markers, and  $\Delta p_L$ : hollow markers. (a) Experiment (I) helium–argon; (b) experiment (II) helium–neon. The error bar shows the standard deviation estimated from the precision of the pressure sensors used in each experiment.

is the mole percentage of helium. The mole fraction of the feed gas is not very accurate due to the limited accuracy of mass flow controllers, but we can obtain the difference of mole percentages obtained by the test device  $\Delta\chi^{(n)}$  ( $n = 1, 2, \dots, 4$ ), which corresponds  $\chi_L - \chi_F$  in the numerical simulation in Section 3, by

$$\Delta\chi^{(n)} = \chi \left[ C_1^{(n)} \right] - \frac{\chi \left[ H_1^{(n+1)} \right] + \chi \left[ H_1^{(n)} \right]}{2}. \quad (10)$$

It is noted that the restriction (5) is achieved only approximately. It takes several hours to carry out process (iv) above, and we observe some deflection of  $p_i$  due to the variations of environmental temperature and pressure during this period. In the case with large volume flux  $Q_i$ , large pressure variation along the flow channels forces us to use pressure sensors with larger full scale, which leads larger difference between the values of  $p_i$  obtained between the calibration and the main experiments. In the cases where we control  $Q_L$  by the length of the tubing, we can only select

best tubing from several sets to satisfy  $Q_L \approx Q_I$ . Therefore, in the following results, we use the average volume flux  $Q$  defined by

$$Q = \frac{Q_I + Q_L}{2},$$

instead of  $Q_I$ .

The results of the experiments are shown in Figs. 12–15. Figure 12 shows the values of  $\Delta\chi$  [average of four  $\Delta\chi^{(n)}$  in (10)] versus  $Q$ . Figure 12(a) shows the result of experiment (I), where the range of volume flux  $Q$  is limited but the experiments are carried out for several temperature differences  $\Delta T = 20, 30$ , and 45 K. The result for experiment (II) is shown in Fig. 12(b), where  $\Delta T$  is fixed to 30 K and the experiments are carried out for a wider range of  $Q$ . In both cases, the value of  $\Delta\chi$  is positive; that is, the smaller gas – helium – is concentrated at the loop part  $H_2 \rightarrow C_1$  as is anticipated by the numerical simulation in Section 3. In experiment (I), the value of  $\Delta\chi$  for a fixed value of  $Q$  increases linearly as  $\Delta T$  increases. The value of  $\Delta\chi$  for given  $\Delta T$  also increases as  $Q$  increases. The value of  $\Delta\chi$  reaches 15% for the case of  $\Delta T = 45$  K and  $Q = 40$  sccm. In experiment (II), the value of  $\Delta\chi$  takes its maximum value around  $Q = 100$  sccm. Since the volumetric porosity of the copper mesh [see Fig. 5(b)] is around 60%, the flow velocity along the membrane is around 0.5 m/s at  $Q = 100$  sccm. These qualitative features of  $\Delta\chi$  match the results of numerical simulation in Section 3. The values of  $\Delta\chi$  is much larger than the variance in four measured values of  $\Delta\chi^{(n)}$ ; the value of  $\max \Delta\chi^{(n)} - \min \Delta\chi^{(n)}$  for each experiment is 0.09% on average. The errors in  $Q$  result from the accuracy of the mass flow controllers  $M_1$  and  $M_2$ , and their total uncertainty is smaller than 3.3 sccm for  $Q \leq 100$  sccm and 29 sccm for  $Q > 100$  sccm.

Figure 13 shows the difference of  $Q_I$  and  $Q_L$  in percentage:

$$Err_Q = 100 \frac{Q_I - Q_L}{Q}.$$

The experiments for  $Q \leq 40$  sccm are carried out by a smaller valve  $V_1$  (SS-SS1), those with  $40 \text{ sccm} < Q \leq 100$  sccm are carried out by a larger valve (SS-2MG). The experiments are carried out without valve  $V_1$  for larger values of  $Q$ . As is shown in the figure, the maximum size of the error is around 7%. In order to confirm that the molecular exchange  $Q^A > 0$  and  $Q^B < 0$  occurs in the device, we calculated  $Q^A$  and  $Q^B$  by

$$Q^A = \chi [C_1] Q_L - \chi [H_1] Q_I,$$

$$Q^B = (1 - \chi [C_1]) Q_L - (1 - \chi [H_1]) Q_I.$$

The results are plotted in Fig. 14. It is clear that helium flows in the direction of  $C \rightarrow H$  through the membrane, while argon or neon flows in the direction of  $H \rightarrow C$ . The size  $Q^A - Q^B$  increases as  $Q$  increases, while the speed of the increase seems to decrease in  $Q > 100$  sccm in Fig. 14(b).

Figure 15 shows the result of the pressure in these experiments. As is described in the previous paragraph, the pressure drop along the system is fairly large for larger values of  $Q$ , and the measurement depends on the location of the pressure sensors. Therefore, we estimated the values of pressure difference at two trenches shown in Fig. 4(b) from the values of  $p_i$  obtained by the sensors,  $Q_I$  and  $Q_L$ , assuming Hagen–Poiseuille flow in the tubing. The result is shown in Fig. 15, where the pressure difference at the trench around  $H_1 - C_2$  ports is denoted by  $\Delta p_i$  and that around  $H_2 - C_1$  ports by  $\Delta p_L$ . The value of  $\Delta p_i$  is close to  $\Delta p_L$  for experiment (I). The value of the pressure difference (around 1 kPa for  $\Delta T = 30$  K) is roughly the same as the value  $p_F - p_R$  expected by numerical simulation for  $m^B/m^A = 10$  and  $T_F/T_R = 1.05$  [see Fig. 8(b)]. On the other hand,  $\Delta p_i$  is fairly larger than  $\Delta p_L$  in experiment (II) at larger flow rate  $Q$ . In this case, the molecular exchange condition (1) is satisfied only on the average over the membrane; each micro-channel does not generally satisfy the molecular exchange condition.

## 5. Discussion

We have analyzed the performance of the device in the preceding two sections, numerically in Section 3 and experimentally in Section 4. These two results are clearly in a good agreement with each other. The fabricated device, however, naturally has various uncertainties. In this section, some of these uncertainties will be discussed with quantitative comparisons of the results.

As for the thermal transpiration performance, the actual temperature difference applied to the MCE membrane is smaller than the temperature difference between the metal plates H and C. The present MCE membrane is a filter product, and we do not know the actual size of pores for the gaseous flow. In the present device, the surface of the membrane is covered by metal meshes, which may change the effective porosity of the membrane. These factors can be estimated from the pressure–flux relation obtained in Section 4.2. Let  $\theta \Delta T$  be the temperature difference applied to the membrane and  $d_{MCE}$  and  $\varepsilon$  be, respectively, the effective pore diameter and porosity of the membrane. From the linear theory of the Boltzmann equation [cf. Eq. (A.2)], the volume flux  $Q^* = Q^A + Q^B$  through the device is given by

$$Q^* = S\varepsilon \frac{d_{MCE}}{t} \sqrt{\frac{2\kappa T_C}{m^A}} \left[ \frac{\theta \Delta T}{T_C} N_T + \frac{\Delta p}{p_C} N_p \right], \quad (11)$$

where  $S$  and  $t$  are, respectively, the area and thickness of the MCE membrane,  $p_C$  is the reference pressure (pressure at  $C_2$ ), and  $N_*$  ( $*$  =  $T, p$ ) are nondimensional functions of the Knudsen number  $\ell_C/d_{MCE}$  ( $\ell_C$ : reference mean free path of A-molecules at number density  $p_C/\kappa T_C$  of molecules). The values of  $N_*$  also depend on gas components, molecular model, and the shape of the cross section of micro-channel. For binary mixture of hard sphere molecules, enough amount of data is available only for the 2D channel [37]. In the case of pure gas, detailed data for various cross sectional shapes including 3D channel are available for BGK and S-model [17,31], which will be used in the following discussion. From the present experimental conditions,  $T_C = 300$  K,  $p_C = 101$  kPa, and  $S = 9.0$  cm<sup>2</sup>. For binary mixture of hard sphere molecules, we use

$$\begin{aligned} \sqrt{\frac{2\kappa T_C}{m^A}} &= 1120 \text{ m/s}, & \ell_C &= 1.70 \times 10^{-7} \text{ m}, \\ m^B/m^A &= 10, & \chi &= 50\% \end{aligned} \quad (12)$$

to express the 50% v/v helium–argon mixture used in the experiment. For BGK and S-model of pure gas, we have to choose appropriate values of  $(m^A, \ell_C)$ , say,  $(m^{BGK}, \ell^{BGK})$ , for present gas mixture. Since the behavior of the gas at intermediate Knudsen numbers is important in the present device, we make use of Knudsen minimum (that is, the value of  $|N_p|$  takes its minimum value at some intermediate Knudsen number). That is, we apply

$$\sqrt{\frac{2\kappa T_C}{m^{BGK}}} = 623 \text{ m/s}, \quad \ell^{BGK} = 3.71 \times 10^{-7} \text{ m}, \quad (13)$$

for the BGK model and

$$\sqrt{\frac{2\kappa T_C}{m^S}} = 619 \text{ m/s}, \quad \ell^S = 2.90 \times 10^{-7} \text{ m}, \quad (14)$$

for the S-model so that these models give the same volume flux  $Q^*$  and diameter  $d_{MCE}$  with the binary mixture of hard sphere gas ( $m^B/m^A = 10$  and  $\chi = 50\%$ ) at Knudsen minimum for the 2D channel.

Since we have the data for  $N_T$  and  $N_p$ , the results of experiment (8) and (9) give the relation among  $\theta$ ,  $d_{MCE}$ , and  $\varepsilon$ . That is, the ratio

of two volume fluxes under  $\Delta p = 0$  and  $\Delta T = 0$  is given by, from (11),

$$\theta \frac{N_T}{N_p} = \frac{Q(\Delta p = 0) \Delta p / p_C}{Q(\Delta T = 0) \Delta T / T_C}.$$

This equation with the results (8) and (9) determines the value of the Knudsen number or the value of  $d_{MCE}$  as a function of  $\theta$ . The value of  $\varepsilon$  is then obtained from (8) and (11). The result is shown in Fig. 16. The panel (a) shows the effective pore diameter  $d_{MCE}$  versus the effective porosity  $\varepsilon$  of the MCE membrane, and panel (b) shows the temperature difference ratio  $\theta$  versus  $\varepsilon$ . The black lines are obtained by using  $N_T$  and  $N_p$  for the 2D channel with binary mixture of hard sphere molecules of  $m^B/m^A = 10$  and mole percentage 50%. The red lines and green symbols [which are almost on the black line in panel (a)] are those with 2D channel results with, respectively, BGK and S-model for pure gas. The blue symbols are also the result of the BGK model but 3D channel shape (square cross section). The similar result for the S-model is also shown in the figure by orange symbols. As the result of conversion (13) and (14), BGK and S-model give almost the same results of  $(\varepsilon, d_{MCE})$  relation with the binary mixture of hard sphere molecules for the 2D case. On the other hand, the difference between 2D and 3D channels is appreciable. Assuming that the conversions (13) and (14) are still valid for the 3D model, we use  $(\varepsilon, d_{MCE}, \theta)$  relation for 3D models to discuss the results of experiments. Since the porosity of MCE membrane, stainless fiber sheet, and copper mesh are, respectively, 0.65, 0.8, and 0.6, the effective porosity  $\varepsilon$  will be in the range of  $0.3 \lesssim \varepsilon \lesssim 0.65$ . Therefore, the effective pore size  $d_{MCE}$  is in the range

$$0.1 \mu\text{m} \lesssim d_{MCE} \lesssim 0.2 \mu\text{m}, \quad (15)$$

from the result for 3D case in Fig. 16(a). This is consistent with the product specifications of our MCE membrane (pore size  $0.1 \mu\text{m}$ ). The above result shows a slightly larger pore size, which can be caused by the cracks created in the fabrication process. The value of  $\theta$ , obtained by 3D data, shows some model dependency but is around

$$\theta \approx 0.3.$$

That is, only 30% of the temperature difference  $\Delta T$  is conducted to the MCE membrane. This is close to the corresponding value in [26], where around 20% of the temperature difference between hot and cold parts is conducted to the MCE membrane. It is possible that the heat conduction is blocked by the presence of the flow channels F and R of height 0.2 mm along the MCE membrane.

Now we discuss the results for the gas separation experiment described in Section 4.3. The gain  $\Delta\chi$  of helium in experiment (I), Fig. 12(a), corresponds to the result of numerical simulation  $\Delta\chi$  in Fig. 8(a). The comparison is done by matching the temperature difference and the pore size of the membrane. Since the temperature difference regarding to the MCE membrane may be  $\theta\Delta T$ , the corresponding value of the temperature ratio in the numerical simulation is  $T_F/T_R = 1 + \theta\Delta T/T_C$ . That is,  $T_F/T_R - 1 \approx 0.02(\Delta T = 20 \text{ K})$ ,  $0.03(\Delta T = 30 \text{ K})$ , and  $0.05(\Delta T = 45 \text{ K})$ . The values of  $\Delta\chi$  for these  $T_F/T_R$  can be estimated from the results in Fig. 8 since  $\Delta\chi$  is almost linear to  $T_F/T_R - 1$  for smaller values of  $v_F/c_R$ ; e.g.,  $\Delta\chi \approx 3\%$  for  $T_F/T_R = 1.03$  and  $\Delta\chi \approx 5\%$  for  $T_F/T_R = 1.05$ . The matching of pore size (15) is complicated, since it is related to the device sizing parameters,  $D/d$ ,  $L/d$ , and  $t/d$  as well as the Knudsen number. The parameters used in Fig. 8 match the fabricated device if  $d_{MCE} = 0.1 \mu\text{m}$ ; in this case the numerical data corresponds to the device with  $D = 0.2 \text{ mm}$ ,  $L = 30 \text{ mm}$ ,  $t = 100 \mu\text{m}$ , and  $\text{Kn} = 2$ . In the case of  $d_{MCE} = 0.2 \mu\text{m}$ , the values of  $D$ ,  $L$ , and  $t$  are doubled and  $\text{Kn} = 1$ . The larger  $D$  and  $t$  may decrease the gain  $\Delta\chi$  of the numerical results, and the larger  $L$  may increase it. Assuming linear dependency of  $\Delta\chi$  on  $1/D$ ,  $1/t$  and  $L$ , the

performance of the fabricated device may be twice of the numerical data in Fig. 8 except the effect of the Knudsen number. The effect of the Knudsen number can be estimated from Fig. 9; the gain for  $\text{Kn} = 1$  may be around 1.5 times larger than that for  $\text{Kn} = 2$ .

According to the above discussion on temperature difference and pore size, the maximum gain  $\Delta\chi$  in experiment (I) at  $\Delta T = 45 \text{ K}$  is estimated to be in the range of 5% ( $d_{MCE} = 0.1 \mu\text{m}$ ) and 15% ( $d_{MCE} = 0.2 \mu\text{m}$ ) from the results of numerical simulation. Figure 9 also shows that the gain  $\Delta\chi$  is almost the same for  $m^B/m^A = 4$  and 10. Therefore, the gain  $\Delta\chi$  in experiment (II), where  $\Delta T = 30 \text{ K}$ , is estimated to be in the range from 3% to 9%. In the experiment (I), as seen from Section 4.3, the value of  $\Delta\chi$  already marks 15% for  $\Delta T = 45 \text{ K}$ , and larger value of  $\Delta\chi$  is expected for larger flux  $Q$ , while the maximum gain for experiment (II) is 7%. It is clear that the  $\Delta\chi$  obtained in the experiment is too large only for helium–argon mixture. There will be many reasons for this disagreement. The 2D shape of micro-channel used in the numerical simulation and the difference of effective porosity of the membrane do not explain the disagreement, since they are common to experiments (I) and (II). One of the reason would be the selection of diameter of the molecules  $d_m^A = d_m^B$  applied in the present numerical simulation. The diameter of molecules, calculated from the viscous coefficient,  $d_m^{\text{Ar}}/d_m^{\text{He}} \approx 1.7$  and  $d_m^{\text{Ne}}/d_m^{\text{He}} \approx 1.2$  [31]. This means that the argon or neon molecules experience more collisions than expected in the simulation. That is, the effective Knudsen number for the experiment is much smaller than  $\text{Kn} = 1$  or 2, and this results in larger  $\Delta\chi$  obtained in the experiment, especially for helium–argon experiment (I).

## 6. Conclusion

In Section 2, we proposed a device that induces the molecular exchange flow through the membrane with the aid of the thermal transpiration. The device accumulates the molecular exchange effect as the gradient of the mole fraction along the membrane. The performance is estimated theoretically in Section 3, where the combination of mass conservation and rarefied gas flow database [37] leads to plausible results. The performance of the fabricated device is tested in Section 4. The results of experiments are in qualitatively good agreement with the theoretical result. That is, the gas component of smaller mass of molecules is concentrated at the loop part between heated and unheated sides of the membrane, the gain of mole percentage  $\Delta\chi$  is almost proportional to the temperature difference, and the value of  $\Delta\chi$  takes its maximum value at some flow speed along the membrane. Furthermore, the quantitative features are also reproduced by the theoretical results. The characteristic values of the device, such as the maximum variation of mole percentage  $\Delta\chi$ , the appropriate flow speed along the membrane for large values of  $\Delta\chi$ , and the pressure difference between the front and rear sides of the membrane  $\Delta p_I$  or  $\Delta p_L$ , remain the same order with these values estimated by the theory in Section 3.

The present device is somewhat similar to the membrane gas separator. Indeed the motion of molecules in the membrane is the key of the device, and some membrane gas separator makes use of the counter flow arrangement as in the present device. However, the molecular transport through the membrane is quite different. In the membrane gas separator, both the molecules of product and residual gas flow in the same direction, and thus the selectivity is quite important. It is also difficult to obtain high purity output. In the present device, molecular exchange – the molecules of product and residual gas flow in the opposite direction – is established. This device is free from the limitation of the selectivity [4], and we do not find the limit on the purity in the numerical simulation. Due to the molecular exchange setup, low cost membranes with larger

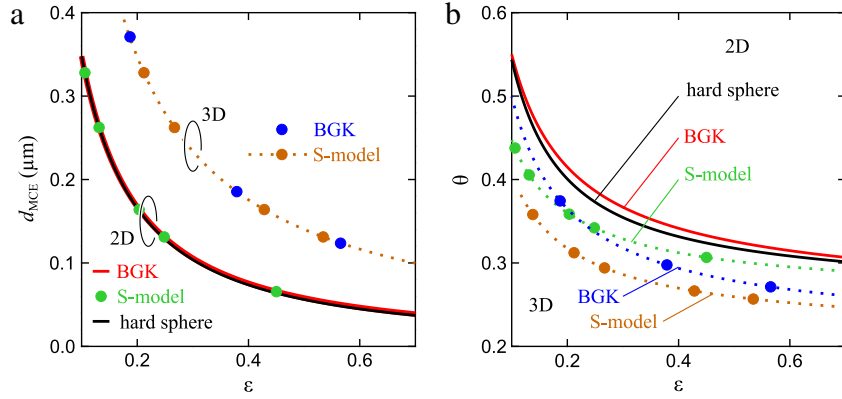


**Fig. 16.** Estimated value of (a) temperature difference ratio  $\theta$  and (b) effective pore diameter  $d_{MCE}$  versus effective porosity  $\varepsilon$ . The results with  $N_T, N_p$  for the 2D channel and the square channel (indicated by 3D in the figure). The black lines are the results with the binary mixture of hard sphere molecules (mass ratio 10 and mole percentage 50%). The red lines and blue symbols are that with BGK model for pure gas. The green and orange symbols are that with S-model for pure gas. The dashed lines indicate the data by spline approximation. (For interpretation of the references to color in this figure legend, the reader is referred to the web version of this article.)

pore size ( $0.1 \mu\text{m}$ ) and thickness ( $110 \mu\text{m}$ ) compared with those used in the membrane gas separation is available.

In view of the flow direction in the membrane, the present method can be considered as a revision of the thermal diffusion column method [39]. In the thermal diffusion column, the small molecules and larger molecules flow in the opposite radial direction due to the temperature and pressure gradient, which is essentially the same as the molecular exchange flow in this paper. The difficulty in the thermal diffusion column is that the effect of molecular exchange is accumulated by the natural convection induced in the longitudinal direction of the column, since the natural convection is characteristic to the gas in the continuum limit while the molecular exchange flow is characteristic to rarefied or molecular gas [6]. In the present device, we also make use of the properties of continuum flow, but they are separated from the molecular exchange flow in the membrane. Therefore, we can choose the local Knudsen number in channel F and R separately from that in the micro-channel.

The present device, however, does not produce concentrated gas. All of the concentrated gas, which flows out the front side of the membrane, flows back to the rear side of the membrane except the small amount of sample gas taken by the gas sampling system. The problem is that the outlet of the residual gas is located close to the inlet for the feed gas (cf. Fig. 1); they are separated only by a single membrane which can maintain small difference of mole percentage. If the separator produces volume flux  $\delta Q_i$  of the gas with increment of mole percentage  $\Delta\chi$  from volume flux  $Q_i$  of feed gas, the conservation of mass leads that the difference of mole percentage between the feed and residual is  $\delta\Delta\chi / (1 - \delta)$  without regard to the values of  $Q^A$  and  $Q^B$  through the membrane. This restricts the value of the production rate  $\delta$  of the present device. This limitation will be removed by more sophisticated constructions, e.g., the cascade connection of units or some reflux process of residual to arrange better positions of the inlet and outlet, which can be found in other methods of gas separation. The construction of such system is left for the future work. Another problem is the energy efficiency, which is not estimated in the present work due to no product gas. In general, we cannot expect too much for the energy efficiency. The heated gas molecules may convey their energy in the random direction, and only a part of the energy is used to induce the thermal transpiration flow. The present device, however, works with small temperature differences around 30 K. Some pressure difference is also required, but it is only a few kilo pascals. It is important that the required pressure difference is the order of the pressure difference that can be induced by the thermal transpiration flow. Therefore, it is expected that this kind of device works under the energy supply of low level external heat only, which would be quite unique compared with other methods of gas separation.

## Acknowledgments

This joint work is initiated by Institutional Program for Young Researcher Overseas Visits #34 by Japan Society for the Promotion of Science (JSPS). The support by JSPS Grants-in-Aid #23560196 is gratefully acknowledged.

## Appendix. Method of solution of numerical simulation

The pipenet method for the numerical model Fig. 6 is described here. The channel # ( $\# = F, R$ ) is sliced into small sections of width  $2d$  in the  $X_1$  direction. The sections are indexed by  $i$  as  $\Omega_{\#(i)}$ ;  $i = -L_-/2d$  for the section at  $X_1 = -L_-$  and  $i = (L + L_+)/2d - 1$  at  $X_1 = L + L_+$ . We calculate the time-variation of the number of  $\alpha$ -molecules in  $\Omega_{\#(i)}$  with the mass conservation. For example, we have

$$\frac{2dD}{\kappa T_F} \frac{P_{F(i)}^{\alpha(k+1)} - P_{F(i)}^{\alpha(k)}}{\Delta\tau} = D \left( F_{F(i-1)}^{\alpha(k)} - F_{F(i)}^{\alpha(k)} \right) + dq_{(i)}^{\alpha(k)} \quad (\alpha = A, B), \quad (\text{A.1})$$

for the part of channel F over the membrane, where  $p_{F(i)}^{\alpha(k)}$  is the partial pressure of  $\alpha$ -gas ( $\alpha = A, B$ ) in  $\Omega_{F(i)}$  at time  $\tau = k\Delta\tau$  ( $k = 1, 2, \dots$ ),  $F_{F(i)}^{\alpha(k)}$  is the molecular flow rate of  $\alpha$ -gas from  $\Omega_{F(i)}$  to  $\Omega_{F(i+1)}$  per unit time and per unit area, and  $q_{(i)}^{\alpha(k)}$  is that through  $i$ th micro-channel in the direction of  $R \rightarrow F$ . The above formulation can be extended to channel R, and the other parts of channels with no micro-channel. The difference equations for channel F and R in the range of  $-L_-/2d + 1 \leq i \leq (L + L_+)/2d - 2$  can be considered as a system of difference equations for  $p_{\#(i)}^{\alpha(k)}$  [ $\# = F, R$ ;  $\alpha = A, B$ ;  $-L_-/2d \leq i \leq (L + L_+)/2d - 1$ ], provided that the flow rates  $q_{(i)}^{\alpha(k)}$  and  $F_{\#(i)}^{\alpha(k)}$  are expressed by  $p_{\#(i)}^{\alpha(k)}$ .

Here we discuss on the expression of  $q_{(i)}^{\alpha(k)}$ . Since the flow in the micro-channel is vanishingly small, the following formula [18–20,37], which is obtained from the linearized Boltzmann equation, can be used for the molecular flow rate  $q^\alpha$  per unit area in a micro-channel:

$$q^\alpha = \bar{n} \sqrt{\frac{2\kappa\bar{T}}{m^\alpha}} \left[ N_T^\alpha \frac{T'}{\bar{T}} + N_p^\alpha \frac{p'}{\bar{p}} + N_\chi^\alpha \frac{\chi'}{100} \right] d, \quad (\text{A.2})$$

where  $\bar{T}$ ,  $\bar{p}$ , and  $\bar{n}$  ( $=\bar{p}/\kappa\bar{T}$ ) are the representative values of temperature, pressure, and number density, respectively; the values emphasized with prime indicate the corresponding gradients along the micro-channel.  $N_*^\alpha$  ( $*$  =  $T, p$ , and  $\chi$ ) are non-dimensional

coefficients that depend on the representative values of Knudsen number  $\overline{\text{Kn}}$ , mole percentage  $\bar{\chi}$ , and the parameters in intermolecular potential model including the mass ratio  $m^B/m^A$ . These coefficients are to be obtained from separate analysis for thermal transpiration, Poiseuille, and diffusion flows through a long tube [15]. Sharipov et al. clarified overall features of these values by making use of model kinetic equation and Onsager–Casimir reciprocity [18–20]. In [37], a database of these coefficients for various intermolecular potentials has been constructed by around  $10^4$  cases of numerical calculations of the same kinetic equation and the supplemental asymptotic analysis for small and large Knudsen numbers. The online version of [37] provides a ready-made computer program of the database; we can obtain the values of  $N_p^\alpha$  as if they were standard mathematical functions on  $\overline{\text{Kn}}$  and  $\bar{\chi}$ . With the aid of this database, the values of  $q_{(i)}^{\alpha(k)}$  are obtained by letting

$$\begin{aligned} T' &\rightarrow \frac{T_F - T_R}{t}, & p' &\rightarrow \frac{\Delta p_{(i)}^{(k)}}{t}, & \chi' &\rightarrow \frac{\Delta \chi_{(i)}^{(k)}}{t}, \\ \bar{T} &\rightarrow \frac{T_F + T_R}{2}, & \bar{p} &\rightarrow \frac{p_{F(i)}^{(k)} + p_{R(i)}^{(k)}}{2}, & \bar{\chi} &\rightarrow \frac{\chi_{F(i)}^{(k)} + \chi_{R(i)}^{(k)}}{2}, \end{aligned}$$

in (A.2), where  $\Delta_{(i)}^{(k)} h$  ( $h = \chi, p$ ) are the difference of mole percentage or pressure between the front and rear sides of the membrane

$$\Delta h_{(i)}^{(k)} = h_{F(i)}^{(k)} - h_{R(i)}^{(k)}, \quad (h = \chi, p).$$

The mole percentage  $\bar{\chi}$  is computed from the ratio of the partial pressure:

$$\chi_{\#(i)}^{(k)} = 100 \frac{p_{\#(i)}^{A(k)}}{p_{\#(i)}^{(k)}}, \quad p_{\#(i)}^{(k)} = p_{\#(i)}^{A(k)} + p_{\#(i)}^{B(k)} \quad (\# = F, R). \quad (\text{A.3})$$

The values of local Knudsen number of each micro-channel,  $\overline{\text{Kn}}$ , are calculated according to each intermolecular potential model with the values of  $\bar{T}$  and  $\bar{p}$  at the  $i$ th micro-channel.

On the other hand, we have no precise data for  $F_{\#(i)}^{\alpha(k)}$ : they are non-vanishing fluxes that may affect the mole fraction downstream (that is, they include the effect of convection terms of fluid dynamic equations), and the channel walls have innumerable holes that may affect flow properties. Here, we assume that they still consist of the part of plane Poiseuille flow proportional to pressure gradient  $p' = dp/dX_1$  and the part of diffusion proportional to  $\chi' = d\chi/dX_1$ , and apply Eq. (A.2) (with the replacement of  $d$  to  $D$ ) to evaluate  $F_{\#(i)}^{\alpha(k)}$  with the aid of finite difference approximation of the derivatives  $p'$  and  $\chi'$ . The coefficient  $N_p^\alpha$  for large values of  $D/d$  may be replaced with the data by plane Poiseuille flow to save CPU time. The viscosity of the mixture with mole percentage  $\bar{\chi}$  is calculated by the data in [34,35,37] with Eqs. (2) and (3). For hard-sphere mixture with the same diameter of molecules, Eq. (4) with the replacement of  $m^A \rightarrow [\bar{\chi}m^A + (100 - \bar{\chi})m^B]/100$  can be used for the viscosity of the mixture; the maximum error of the viscosity is around 0.3 ( $m^B/m^A - 1$ )% for  $m^B/m^A = 2, 4$ , and 10.

The difference equation Eq. (A.1) is of diffusion type, since  $F_{\#(i)}^{\alpha(k)}$  is expressed by the difference of  $p_{\#(i+1)}^{\alpha(k)}$  and  $p_{\#(i)}^{\alpha(k)}$ . Therefore we need two boundary conditions for each channel and gas component. These eight conditions are given by (i) total pressures  $p = p^A + p^B$  at inlet of F ( $p = p_F$ ) and outlet of R ( $p = p_R$ ), (ii) the value  $\chi_F$  of mole percentage at inlet of channel F, (iii) two conditions  $d\chi/dX_1 = 0$  at the outlets of F and R, (iv) pressure drop  $p_D$  between the outlet of F and inlet of R, and (v) the mass conservations for A and B gas between the exit of channel F inlet of channel R. The system of difference equations with above eight boundary conditions determines the distributions of partial pressures  $p_{\#(i)}^{\alpha(k+1)}$  [ $\# = F, R; \alpha = A, B; -L_-/2d \leq i \leq (L + L_+)/2d - 1$ ]

at time  $\tau = \Delta\tau(k + 1)$  from those at  $\tau = \Delta\tau k$ . The process is repeated until we obtain the steady distribution of partial pressures  $p_{\#(i)}^{\alpha(k)}$  along channels F and R. Then the distributions of steady mole percentage  $\chi_{\#(i)}^{(k)}$  in Fig. 7 are calculated by (A.3). In the numerical calculation, we rewrite explicit form of the difference equation (A.1) for  $p^\alpha$  into the implicit form for  $p^A$  and  $p$  to obtain the steady solution quickly with no restriction of the CFL condition. In order to reduce the access to the database of  $N_p^\alpha$ , the values of  $q_{(i)}^{\alpha(k)}$  of  $M$  channels nearby are replaced by those of a representative channel.

## References

- [1] W.J. Koros, G.K. Fleming, Membrane-based gas separation, *J. Membr. Sci.* 83 (1993) 1–80.
- [2] P. Pandey, R.S. Chauhan, Membranes for gas separation, *Prog. Polym. Sci.* 26 (2001) 853–893.
- [3] R.W. Baker, Future directions of membrane gas separation technology, *Ind. Eng. Chem. Res.* 41 (2002) 1393–1411.
- [4] L.M. Robeson, W.F. Burgoyne, M. Langsam, A.C. Savoca, C.F. Tien, High performance polymers for membrane separation, *Polymers* 35 (1994) 4970–4978.
- [5] Y. Sone, Flows induced by temperature fields in a rarefied gas and their ghost effect on the behavior of a gas in the continuum limit, in: *Annual Review of Fluid Mechanics*, vol. 32, Annual Reviews, Palo Alto, 2000, pp. 779–811.
- [6] H. Sugimoto, A. Shinotou, Gas separator with thermal transpiration in a rarefied gas, in: D.A. Levin, I.J. Wysong, A.L. Garcia (Eds.), *Rarefied Gas Dynamics*, in: AIP Conference Proceedings, vol. 1333, AIP, 2011, pp. 784–789.
- [7] Y. Sone, M. Yoshimoto, Demonstration of a rarefied gas flow induced near the edge of a uniformly heated plate, *Phys. Fluids A* 4 (1997) 419–440.
- [8] H. Sugimoto, Y. Sone, Vacuum pump without a moving part driven by thermal edge flow, in: M. Capitelli (Ed.), *Rarefied Gas Dynamics*, in: AIP Conference Proceedings, vol. 762, AIP, 2005, pp. 419–440.
- [9] M.N. Kogan, V.S. Galkin, O.G. Friedlander, Stress produced in gases by temperature and concentration inhomogeneities. New type of free convection, *Sov. Phys. Usp.* 19 (1976) 420–438.
- [10] J.C. Maxwell, On stresses in rarefied gases arising from inequalities of temperature, *Philos. Trans. R. Soc. Lond.* 170 (1879) 231–256.
- [11] O. Reynolds, On certain dimensional properties of matter in the gaseous state, *Philos. Trans. R. Soc. Lond.* 170 (1879) 727–845.
- [12] W.H. Keesom, J. Schweers, Some measurements on thermomolecular pressure ratios in hydrogen and in neon, *Physica* 8 (1941) 676–689.
- [13] S.C. Liang, Some measurements of thermal transpiration, *J. Appl. Phys.* 22 (1951) 148–153.
- [14] G.D. Arney Jr., A.B. Bailey, Effect of temperature on pressure measurements, *AIAA J.* 1 (1963) 2863–2864.
- [15] V.G. Chernyak, V.V. Kalinin, P.E. Suetin, The kinetic phenomena in nonisothermal motion of a binary gas mixture through a plane channel, *Int. J. Heat Mass Transfer* 27 (1984) 1189–1196.
- [16] Y. Sone, K. Sawada, H. Hirano, A simple experiment on the strength of thermal creep flow of a rarefied gas over a flat wall, *Eur. J. Mech. B Fluids* 13 (1994) 299–303.
- [17] F. Sharipov, Non-isothermal gas flow through rectangular microchannels, *J. Micromech. Microeng.* 9 (1999) 394–401.
- [18] F. Sharipov, D. Kalempa, Gaseous mixture flow through a long tube at arbitrary Knudsen numbers, *J. Vac. Sci. Technol. A* 20 (2002) 814–822.
- [19] S. Naris, D. Valougeorgis, D. Kalempa, F. Sharipov, Gaseous mixture flow between two parallel plates in the whole range of the gas rarefaction, *Physica A* 336 (2004) 294–318.
- [20] S. Naris, D. Valougeorgis, D. Kalempa, F. Sharipov, Flow of gaseous mixtures through rectangular microchannels driven by pressure, temperature, and concentration gradients, *Phys. Fluids* 17 (2005) 100607.
- [21] F. Sharipov, G. Bertoldo, Poiseuille flow and thermal creep based on the Boltzmann equation with the Lennard-Jones potential over a wide range of the Knudsen number, *Phys. Fluids* 21 (2009) 067101.
- [22] F. Sharipov, V. Seleznev, Data on internal rarefied gas flows, *J. Phys. Chem. Ref. Data* 27 (1998) 657–706.
- [23] F. Sharipov, Data on the velocity slip and temperature jump on a gas–solid interface, *J. Phys. Chem. Ref. Data* 40 (2011) 023101.
- [24] F. Sharipov, Gaseous mixtures in vacuum systems and microfluidics, *J. Vac. Sci. Technol. A* 31 (2013) 050806.
- [25] M. Knudsen, Eine revision der gleichgewichtsbedingung der gase. Thermische molekularströmung, *Ann. Phys. Leipzig* 31 (1910) 205–229.
- [26] N.K. Gupta, Y.B. Gianchandani, Thermal transpiration in mixed cellulose ester membranes: enabling miniature, motionless gas pumps, *Micropor. Mesopor. Mat.* 142 (2011) 535–541.
- [27] F. Sharipov, D. Kalempa, Separation phenomena for gaseous mixture flowing through a long tube into vacuum, *Phys. Fluids* 17 (2005) 127102.

- [28] S. Takata, H. Sugimoto, S. Kosuge, Gas separation by means of Knudsen compressor, *Eur. J. Mech. B Fluids* 26 (2007) 155–181.
- [29] H. Sugimoto, M. Hibino, Numerical analysis on gas separator with thermal transpiration in micro channels, in: M. Mareschal, A. Santos (Eds.), *Rarefied Gas Dynamics*, in: AIP Conference Proceedings, vol. 1501, AIP, New York, 2012, pp. 794–801.
- [30] H. Sugimoto, M. Hibino, Gas separator with thermal transpiration in micro-channels II, *J. Japan Soc. Fluid Mech.* 31 (2012) 495–498.
- [31] Y. Sone, *Molecular Gas Dynamics*, Birkhäuser, Boston, 2007.
- [32] S. Kadowaki, H. Sugimoto, Rarefied gas flow induced by temperature field of multilayer mesh, Special Issue, *J. Japan Soc. Fluid Mech.* 29 (2010) 455–459. (in Japanese).
- [33] H. Sugimoto, S. Kawakami, K. Moriuchi, Rarefied gas flows induced through a pair of parallel meshes with different temperatures, in: T. Abe (Ed.), *Rarefied Gas Dynamics*, in: AIP Conference Proceedings, vol. 1084, AIP, New York, 2009, pp. 1021–1026.
- [34] S. Takata, S. Yasuda, K. Aoki, T. Shibata, Various transport coefficients occurring in binary gas mixtures and their database, in: A.D. Ketsdever, E.P. Muntz (Eds.), *Rarefied Gas Dynamics*, in: AIP Conference Proceedings, vol. 663, AIP, New York, 2003, pp. 106–113.
- [35] E.L. Tipton, R.V. Tompson, S.K. Loyalka, Chapman–Enskog solutions to arbitrary order in Sonine polynomials II: Viscosity in a binary, rigid-sphere, gas mixture, *Eur. J. B. Mech. B/Fluids* 28 (2009) 335–352.
- [36] F. Ahmad, K.K. Lau, A.M. Shariff, G. Murshid, Process simulation and optimal design of membrane separation system for CO<sub>2</sub> capture from natural gas, *Comput. Chem. Eng.* 36 (2012) 119–128.
- [37] S. Kosuge, S. Takata, Database for flows of binary gas mixtures through a plane microchannel, *Eur. J. Mech. B Fluids* 27 (2008) 444–465.
- [38] G.A. Bird, *Molecular Gas Dynamics and the Direct Simulation of Gas Flows*, Clarendon, Oxford, 1994.
- [39] K.E. Grew, T.L. Ibbs, *Thermal Diffusion in Gases*, Cambridge U.P., Cambridge, 1952.